Carbon Structures with Three-Dimensional Periodicity at Optical Wavelengths

Anvar A. Zakhidov,* Ray H. Baughman,* Zafar Iqbal, Changxing Cui, Ilyas Khayrullin, Socrates O. Dantas, Jordi Marti, Victor G. Ralchenko

Porous carbons that are three-dimensionally periodic on the scale of optical wavelengths were made by a synthesis route resembling the geological formation of natural opal. Porous silica opal crystals were sintered to form an intersphere interface through which the silica was removed after infiltration with carbon or a carbon precursor. The resulting porous carbons had different structures depending on synthesis conditions. Both diamond and glassy carbon inverse opals resulted from volume filling. Graphite inverse opals, comprising 40-angstrom-thick layers of graphite sheets tiled on spherical surfaces, were produced by surface templating. The carbon inverse opals provide examples of both dielectric and metallic optical photonic crystals. They strongly diffract light and may provide a route toward photonic band-gap materials.

The creation of structures having large unit cells has been long recognized as a promising way to obtain novel properties. However, despite major interest in new forms of carbon, the unit cell parameters for available carbon crystals do not exceed a few nanometers. If these periodicities could be increased by two orders of magnitude, light waves could interact coherently by diffraction from these long periodicities, like electron waves do in ordinary crystals. The result would be a form of carbon that is an optical photonic crystal. Evidence for such optical photonic crystals would be the occurrence of opalescence due to the Bragg diffraction of light. If the variation in refractive index over the unit cell were sufficiently large, an energy range could exist in which light can be neither emitted nor propagated. Such photonic band-gap crystals provide the optical analogue of semiconductor crystals (*1*–*3*).

The goal of this work is to make carbon photonic crystals for optical wavelengths. Like diamond and the C_{60} fullerene, the targeted carbon photonic crystals are cubic. However, the unit cell for a hypothetical optical photonic crystal based on a fullerene-like carbon would contain >10 million carbon atoms, versus 8 million for diamond and 240 million for C_{60}. Between a few nanometers and about 10 μm, there exists a gap in current ability to fabricate structures that are three-dimensionally periodic. The targeted structures lie in this "fabrication gap." Exciting advances have been made here recently in the assembly of opal-like crystals (*4*, *5*), infiltration of opals (*6*), and formation of periodic oxide foams from either polystyrene lattices or emulsions (*7*). However, neither carbon phases nor insulator-free electrical conductors of any type have been made that are three-dimensionally periodic on the scale of optical wavelengths.

Previously known optical photonic crystals of other materials, such as natural opal, have an atomic level structure that is unrelated to the crystal structure at optical wavelengths. On the opposite extreme, we want to create an optical photonic crystal in which the atomic scale structure is strongly correlated with the crystal periodicity at optical wavelengths. This is challenging, because it requires that a large-scale periodicity dictates a local structural arrangement at a thousand times smaller scale.

Synthesis Concept

Guidance for this process is found in nature, where silica opals are made by self-assembly of SiO_2 spheres into faulted face-centered-cubic (fcc) crystals (*8*). In the natural process, these sphere arrays are infiltrated with hydrated silica having a different refractive index than the SiO_2 spheres. Our process differs in that we infiltrate porous SiO_2 sphere arrays (Fig. 1A) with either carbon or a material that converts to carbon. Also, before this infiltration, we use sintering to create necks between spheres. These necks provide the intersphere interconnections that allow SiO_2 spheres to be chemically removed after infiltration. We call the resulting product an inverse opal, because the voids of the original opal provide the only occupied space.

The above step of generating an extended interface between SiO_2 spheres is critical for producing inverse opals if the infiltrated material completely covers the internal surface

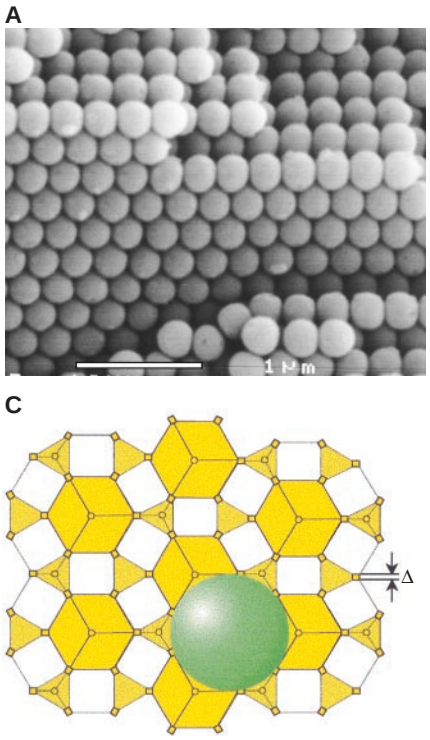

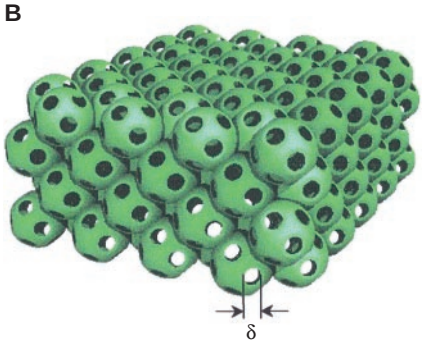

Fig. 1. Opal and inverse opal structures. (**A**) SEM of a porous SiO_2 opal. (**B**) Continuum structural model for a surface-templated inverse opal. (**C**) Schematic representation of interconnected octahedral and tetrahedral void spaces for an inverse opal. Location of the pictured sphere from the original opal structure indicates relationship between direct and inverse opal structures. Dimensions Δ and δ indicate diameters of the interconnections between void spaces for direct and inverse opal structures, respectively.

A. A. Zakhidov and I. Khayrullin are at AlliedSignal, Incorporated, Research and Technology, Morristown, NJ 07962–1021, USA, and in the Department of Thermal Physics of the Uzbekistan Academy of Sciences, Katartal 28, Tashkent, Uzbekistan. R. H. Baughman, Z. Iqbal, C. Cui, and J. Marti are at AlliedSignal, Incorporated, Research and Technology, Morristown, NJ 07962–1021, USA. S. O. Dantas is in the Departamento de Física, Universidade Federal de Juiz de Fara, Juiz de Fora, 36036-330, MG, Brazil. V. G. Ralchenko is at the General Physics Institute, Russian Academy of Sciences, 38 Vavilova Street, 117942 Moscow, Russia.

*To whom correspondence should be addressed. E-mail: anvar.zakhidov@alliedsignal.com and ray.baughman@alliedsignal.com

of the silica opal. Although sintering provides the intersphere interface through which the SiO_2 can be removed after infiltration, too much sintering prohibits infiltration by closing the passages between the octahedral and tetrahedral voids in the original silica lattice. If the sintering provides SiO_2 spheres of diameter D = 250 nm, which are separated by a shorter distance d, simple calculations indicate the narrow range of D/d that is compatible with both the infiltration and the extraction processes. The narrowest channel constriction between octahedral and tetrahedral void spaces (Fig. 1, B and C) occurs on the (111) plane midway between six surrounding spheres and has a diameter $\Delta = 2(3)^{-1/2}d - D$ (which is 39 nm if D/d is unity and zero if D/d is >1.155). With increasing D/d between 1 and 1.155, the diameter of the circular interface between nearest-neighbor spheres [$\delta = (D^2 - d^2)^{1/2}$] increases from 0 to 125 nm.

The infiltration step either completely fills the void volume of the porous silica opal or coats the surfaces of the void space, thereby resulting (after silica extraction) in either a volume-templated inverse opal or a surface-templated inverse opal. Both types of carbon phases consist of an assembly of interconnected tetrahedrally and octahedrally shaped motifs (with eight tetrahedrons and four octahedrons in the cubic unit cell), which are replicas of the void space in the opals (Fig. 1C). These motifs are solid for an ideal volume-templated inverse opal, so the carbon phase consists of a single void network. On the other hand, these motifs are hollow for the surface-templated inverse opals, so there can be two separate three-dimensional void networks (one internal to the octahedral and tetrahedral motifs and the other internal to the array of interconnected hollow spheres).

Silica Opal Templates

The porous silica opals used as templates were made according to published methods used by the jewelry industry to fabricate gem-quality synthetic opal (*5, 8–10*). The SiO_2 spheres were formed by the sodium silicate route (*9, 10*). Spheres made by this process are commercially available from Nissan Chemicals Company. Because the sodium silicate process results in spheres that are polydispersed in sphere diameter, they must be fractionated according to size by repeated sedimentation and redispersion (*9*). The spheres used in this investigation ranged from 150 to 300 nm in diameter.

The growth of SiO_2 opals was by slow crystallization of the monodispersed aqueous colloid at ambient (10 months in a 1-m-long glass cylinder). The resulting deposits were polycrystalline but contained long rod-like single crystals (typically a few centimeters long in the [111] rapid growth direction and a few millimeters in lateral dimensions). Postcrystallization sintering (after drying at 120°C for 2 to 3 days) by thermal annealing (typically for several hours at 700° to 750°C) produced D/d ratios of about 1.035 to 1.055. Mechanical strength measurements indicated when the sintering was sufficient for development of the

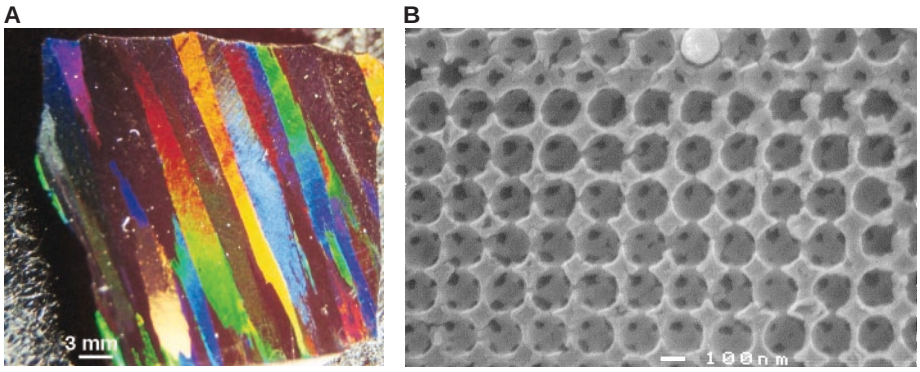

Fig. 3. Inverse opal of graphite produced by the CVD process. (**A**) Photograph showing brilliant opalescence of a polycrystalline plate of graphitic carbon inverse opal based on 300-nm hollow spheres. Long axis direction of the crystallites corresponds to the [111] growth direction of the original SiO_2 opal. (**B**) SEM of a fracture surface of a graphitic carbon inverse opal based on 200-nm hollow spheres. Residual silica sphere in the upper part indicates a rare instance when a sphere survived the silica extraction process. The probable reason this SiO_2 sphere survived is that there were no interconnects with neighboring spheres, so the aqueous HF had no access to this sphere.

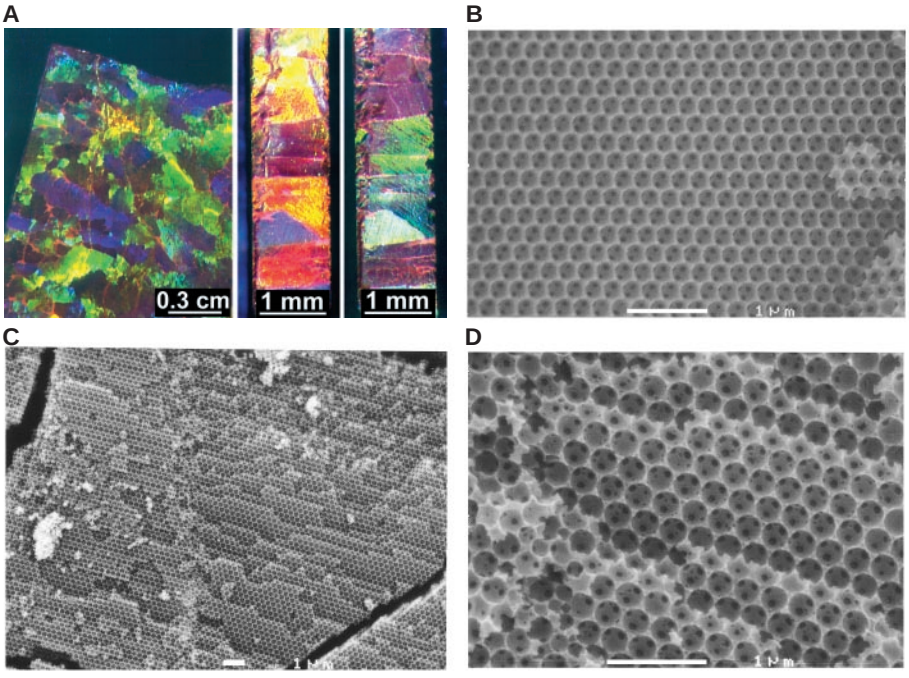

Fig. 2. Glassy carbon and phenolic inverse opals. (**A**) Photographs of intense opalescence of phenolic inverse opal due to Bragg scattering from the three-dimensionally periodic lattice: left, phenolic plate; middle and right, fracture surface orthogonal to the plate for two different illumination angles. Fracture surface corresponds to the left upper edge of opal plate shown at left. Change in color with illumination angle indicates that the color results from diffraction. Pictured opalescence throughout the fracture surface indicates that periodicity of the phenolic inverse opal extends through the millimeter sample thickness. (**B**) SEM of a (111) fracture surface of the phenolic inverse opal shown in (A). (**C** and **D**) SEMs (at two different magnifications) of a (111) fracture surface of a glassy carbon inverse opal derived by carbonizing a phenolic infiltrated SiO_2 opal before extracting the SiO_2. Low magnification image in (C) shows existence of a periodic structure over about 30 layers parallel to the plane of the picture and about 100 layers orthogonal to the cleavage plane. SEMs taken at different positions on the fracture surface indicate that the periodic structure of the glassy carbon inverse opal is maintained over the entire millimeter sample thickness. Cracks originate from boundaries between crystallites. Randomly introduced holes evident in (D) (distinct from the periodic holes arising from intersphere connections) indicate that the volume change on pyrolysis introduces porosity in the glassy carbon if the carbonizing phenolic is not free to decrease lattice dimension.

required intersphere interfaces. Resulting mechanical properties in compression for polycrystalline centimeter-sized cubes of sintered 250-nm-diameter opal spheres typically were a modulus of 24 GPa, an ultimate strength of 107 MPa, and a failure strain of 0.8%. The absence of oversintering (leading to void interconnect closure) was confirmed by observing the transformation from the initial chalk-like appearance to a transparent, opalescent appearance when the opal was submersed in a liquid with about the same refractive index as the SiO_2 spheres (1.42). This relatively high refractive index is consistent with these spheres being substantially void-free. Electron microscopy indicates that these spheres (sliced 70 nm thick) are not significantly porous down to the measurement limit of a few angstroms.

Glassy Carbon Inverse Opals by a Phenolic Route

Carbon inverse opals were fabricated by infiltrating millimeter-thick silica opal plates with a phenolic resin, thermally curing this resin at low temperature, cutting the opal from the phenolic resin, removing residual surface phenolic by oxygen plasma etching, dissolving the SiO_2 from the infiltrated opal with aqueous HF, and pyrolyzing the resulting phenolic inverse opal at progressively increasing temperatures up to 1000°C (*11*). X-ray diffraction data indicate an amorphous structure consistent with a glassy carbon. As expected for a photonic crystal with a large void volume, both the unpyrolyzed phenolic inverse opals and the glassy carbon inverse opals are intensely opalescent (Fig. 2A). This opalescence shifts from predominantly red in the SiO_2 opal (based on 300-nm spheres) to predominantly green-blue in the phenolic inverse opal (Fig. 2A, plate view) and to predominantly dark blue/violet in the final carbon inverse opal (reflecting a 20% or higher contraction in unit cell dimension upon pyrolysis of the phenolic inverse opal as well as refractive index changes). Scanning electron micrographs (SEMs) of fracture surfaces show a highly periodic structure throughout the volume of the unpyrolyzed phenolic inverse opal (Fig. 2B) and the glassy carbon inverse opal obtained by pyrolysis. The void structure consists of an fcc arrangement of spherical voids, each of which is interconnected with 12 neighboring spherical voids through interconnects δ, which can be as small as a few hundred angstroms in diameter *d*. If pyrolysis is done before extraction of the SiO_2 spheres (Fig. 2, C and D), the periodic wall structure of the glassy carbon inverse opal becomes porous (due to the volume change associated with pyrolysis).

Graphitic Carbon Inverse Opals by Chemical Vapor Deposition (CVD)

We also made graphitic inverse opals by CVD on 1-mm-thick opal slabs with a 1:3

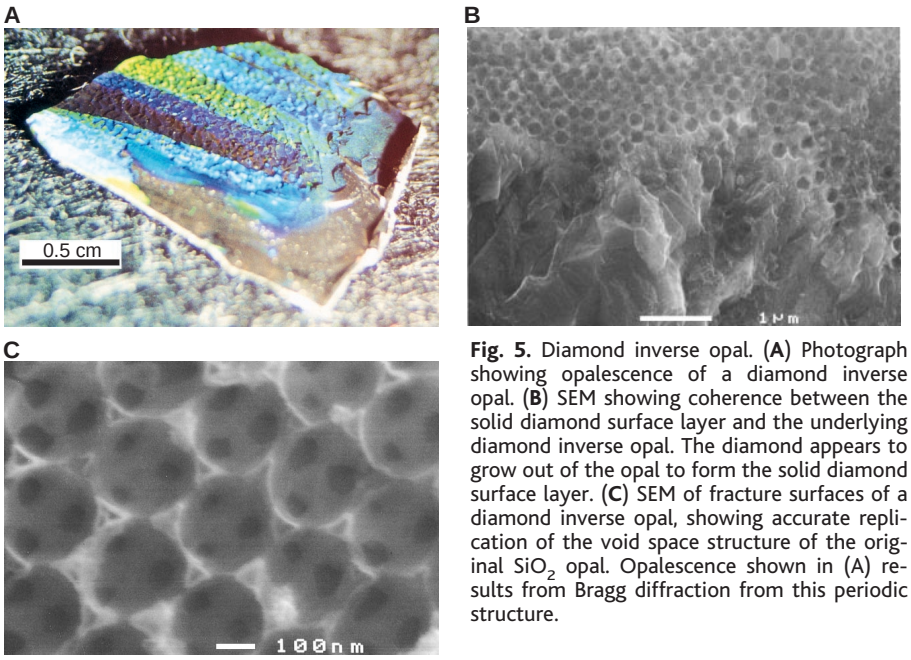

Fig. 5. Diamond inverse opal. (**A**) Photograph showing opalescence of a diamond inverse opal. (**B**) SEM showing coherence between the solid diamond surface layer and the underlying diamond inverse opal. The diamond appears to grow out of the opal to form the solid diamond surface layer. (**C**) SEM of fracture surfaces of a diamond inverse opal, showing accurate replication of the void space structure of the original SiO_2 opal. Opalescence shown in (A) results from Bragg diffraction from this periodic structure.

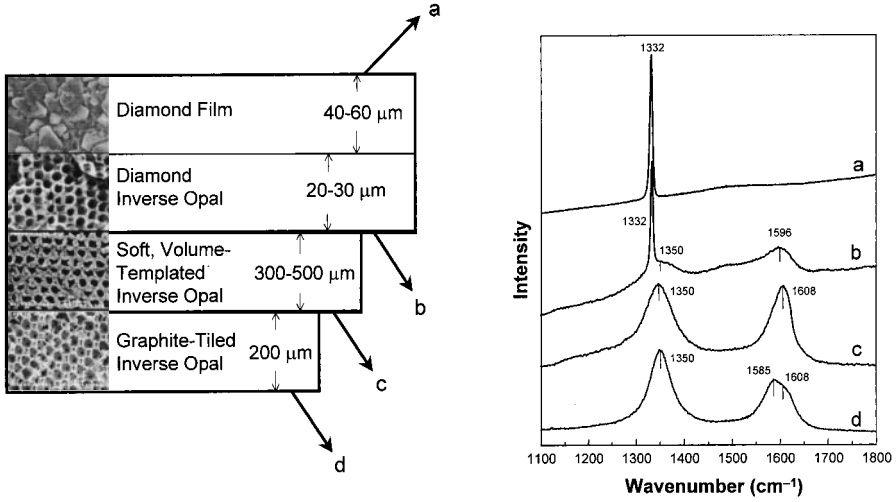

Fig. 4. Schematic edge view of the layers of inverse opal produced by plasma-enhanced CVD, along with SEMs (plate surface for diamond overcoat and perpendicular fracture surfaces for inverse opals) (**left**), and a micro-Raman spectrum (excitation, 514.5 nm; beam diameter, 1 μm) for each layer (**right**). Graphite-tiled inverse opal and volume-templated inverse opal layers were easily separated from overlying layers, which is schematically indicated by the layer recesses (left). Letters indicate the location in these recesses where the corresponding Raman spectra were obtained. The volume-templated inverse opal appears to be easily deformed, which is suggested by the partial collapse of the cavities in the corresponding fracture surface micrograph. Raman spectra for the solid diamond overcoat layer (line at 1332 cm^{-1}) indicates high-quality diamond. Consistent with the electron diffraction data and the coherent intergrowth with the solid diamond layer, Raman spectrum b (right) (with diamond line at 1332 cm^{-1}) indicates that the inverse opal is also composed of diamond. This diamond signature is not from trace quantities of the 2- to 5-nm seed used for diamond growth, because the small size of the seeds results in a very broad line that is downward shifted to about 1323 cm^{-1} (*15*). Broad lines at 1350 and 1596 cm^{-1} indicate that sp^2 carbons are also present, which probably reflects the proximity of this examined surface b to the underlying volume-templated inverse opal containing sp^2 carbons, whose Raman spectrum is curve c. Raman spectrum (curve d) for the graphite-tiled inverse opal is consistent with the presence of small graphite sheets, which is also indicated by electron microscopy (Fig. 7C). The line at about 1585 cm^{-1} is the carbon-carbon stretching mode for graphite sheets and the lines at 1350 and 1608 cm^{-1} are likely Brillouin zone boundary modes (Raman inactive for single-crystal graphite), which arise because of small crystallite size.

molar ratio of propylene and N_2 as the feed gas (1 atm for 6 hours at 800°C) followed by silica removal with aqueous HF. The CVD-produced carbon inverse opal is intensely opalescent (Fig. 3A) and highly periodic and structurally regular down to the 10-nm scale (Fig. 3B). Both the CVD and phenolic processes produced carbon inverse opals that are highly conducting, providing a four-point probe electrical conductivity of about 10 S/cm for inverse opals derived from 200- to 300-nm-diameter SiO_2 spheres. Also, the carbon inverse opals made by both of these processes are stable for hours at >2000°C in inert atmosphere. The major observed Raman lines (at 1349 and 1578 cm^{-1}) indicate finite crystallite-sized graphite in CVD-obtained samples. These lines sharpen, and the line at 1585 cm^{-1} (which is the only Raman-allowed line in this frequency range for single-crystal graphite) increases in relative intensity after the graphitic inverse opal is annealed for 2 hours at 2000°C in an inert atmosphere.

Diamond Inverse Opals by Plasma-Enhanced CVD

Millimeter-thick opal plates were seeded with 2- to 5-nm diamond particles (which serve as nuclei for diamond growth) and carbon was deposited inside the opal plates from a plasma containing hydrogen and methane (*12, 13*). Extraction of the SiO_2 balls from the carbon-infiltrated opal (using aqueous HF) resulted in a material whose structure depends on the proximity to the exterior surface of the original opal plate, which is shown schematically in Fig. 4, left. About a 40- to 60-μm-thick layer of cubic diamond (containing micrometer-sized crystallites with typical diamond crystal morphology) exists on the exterior surface of the opal that was closest to the plasma. The carbon inverse opal closest to this surface is a 20- to 30-μm-thick layer arising from essentially complete filling of the porous opal with ordinary cubic diamond [identified by the electron diffraction pattern and a strong line at the expected position (*14, 15*), 1332 cm^{-1}, in the micro-Raman spectra of Fig. 4, right]. The intense opalescence of the diamond inverse opal (Fig. 5A) indicates that it is a photonic crystal. As is the case for the phenolic and CVD graphite inverse opals, quantitative measurements of Bragg diffraction for the diamond inverse opals provide a lattice constant that is consistent with SEM results. Despite the fact that poor adhesion is typically a problem in diamond coating technology, we find that the exterior diamond layer is intimately connected to the diamond inverse opal (Fig. 5B). SEMs (Fig. 5, B and C) show that the lattice of interconnected octahedral and tetrahedral voids of the starting opal is replicated in the structure of the diamond inverse opal. The 300- to 500-μm-thick layer immediately below the diamond inverse opal (Fig. 4, left) is a volume-templated inverse opal (or a heavily filled surface-templated inverse opal) consisting of a mechanically soft carbon, which tends to separate from the diamond inverse opal layer during SiO_2 extraction.

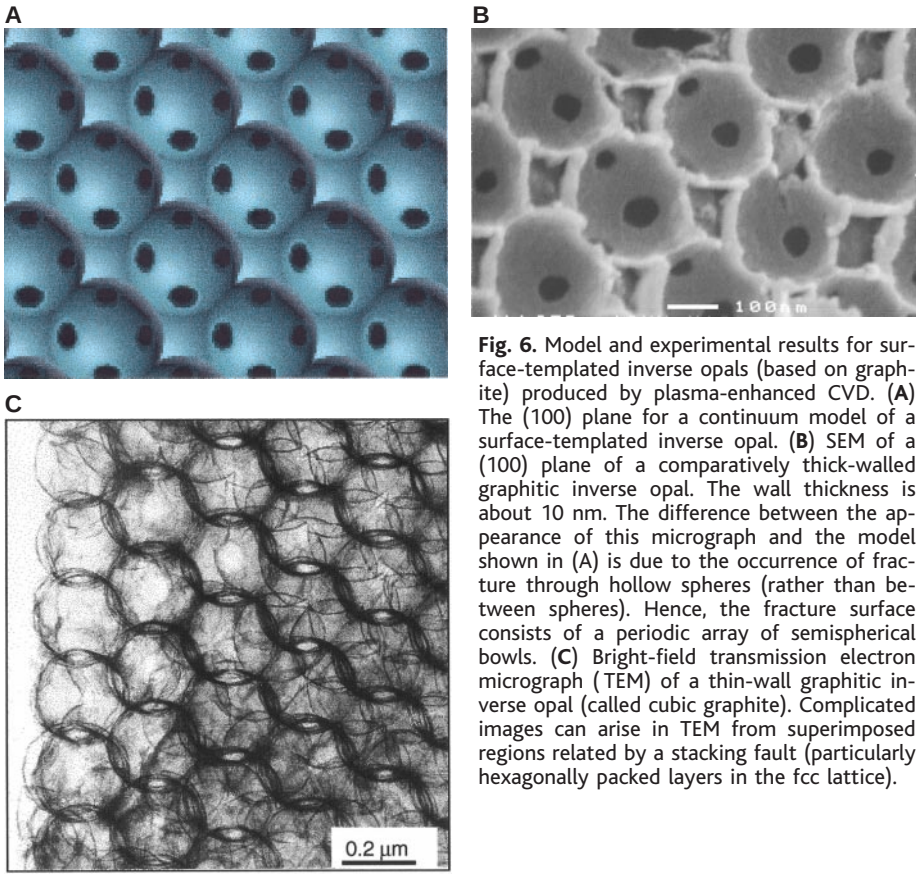

Fig. 6. Model and experimental results for surface-templated inverse opals (based on graphite) produced by plasma-enhanced CVD. (**A**) The (100) plane for a continuum model of a surface-templated inverse opal. (**B**) SEM of a (100) plane of a comparatively thick-walled graphitic inverse opal. The wall thickness is about 10 nm. The difference between the appearance of this micrograph and the model shown in (A) is due to the occurrence of fracture through hollow spheres (rather than between spheres). Hence, the fracture surface consists of a periodic array of semispherical bowls. (**C**) Bright-field transmission electron micrograph (TEM) of a thin-wall graphitic inverse opal (called cubic graphite). Complicated images can arise in TEM from superimposed regions related by a stacking fault (particularly hexagonally packed layers in the fcc lattice).

Graphite-Tiled Inverse Opals (Cubic Graphite)

The innermost layer in the infiltrated carbon of the above samples consists of about 200-μm-thick sheets of an unusual type of graphitic foam (Figs. 6 and 7), which results from coating of the SiO_2 spheres with carbon. The thickness of this coating depends on deposition conditions (compare Fig. 6, B and C) and generally decreases with increasing separation from the infiltration surface. However, a layer thickness of 40 Å is typical for the innermost structure. The void structure of the original opal is precisely replicated in the carbon phase, indicating that these 40 Å thick layers are sufficiently strong to survive the stresses generated during dissolution of the SiO_2 spheres. Most interestingly, the electron micrographs of Fig. 7 show that these very thin layers consist of graphite sheets that are preferentially oriented parallel to the void surface created by removal of the SiO_2 spheres. Hence, the location and curvature of the graphite plane stacks depend on an opal-derived periodicity that is a thousand times longer than the graphite interlayer separation. An electron diffraction pattern from the carbon foam provides diffraction spacings reminiscent of ordinary graphite: 3.43 Å for (002), 2.10 Å for (100), 1.72 Å for (004), and 1.23 Å for (110). As expected, because of the nested layer type of structure, the absence of reflections other than (hk0) or (00l) indicates that the carbon layers are not in lateral registry. This increases the intersheet separation compared with a single-crystal graphite. Covalent bonding between hollow spheres is indicated by the fracture mechanism of this and our other carbon inverse opals: fracture occurs across the sphere centers (Fig. 6B) rather than across intersphere necks as in Fig. 6A. This is like the usual fracture mechanism (*8*) of gem-quality natural opal (but opposite that of our sintered porous opals).

If the channels to neighboring spheres and structural defects are ignored, the graphite-tiled spheres in the carbon phase are similar to a nested arrangement of giant fullerene spheres. There are about 6 million atoms in each sphere layer (based on 250-nm spheres having 60-nm-diameter intersphere channels as in Fig. 6C). Consequently, the unit cell (which has the same $Fm\bar{3}m$ space group and lattice parameter as the original opal) contains about 300 million carbon atoms in a 40 Å thick stack.

In contrast to the case for other carbon photonic crystals that we have described here, the atomic-level arrangement of graphite sheets is a function of the cubic structure existing at optical wavelengths. Consequent-

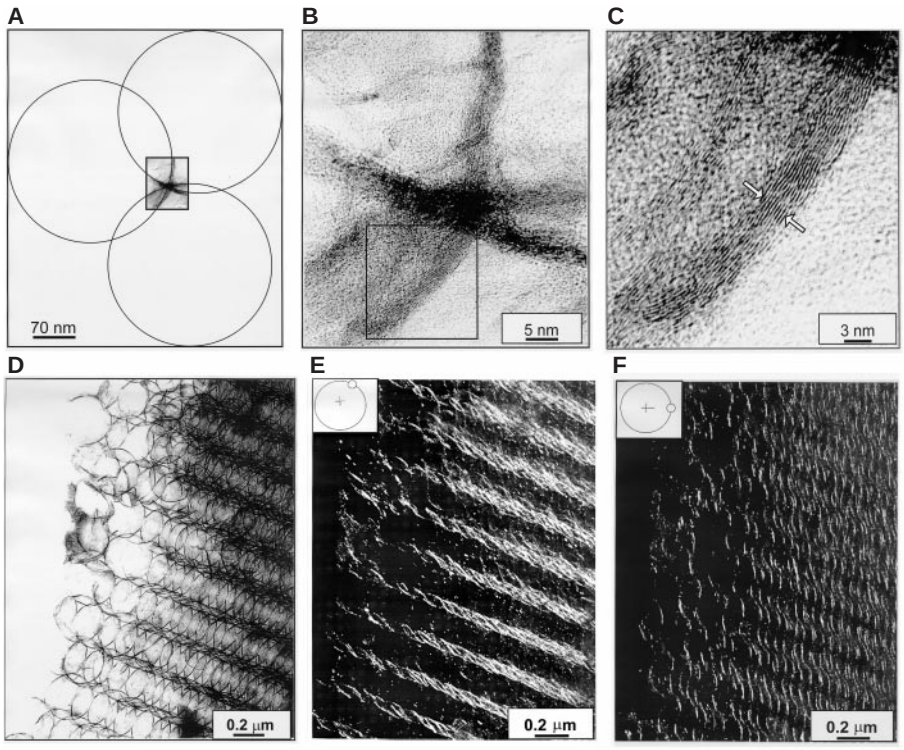

Fig. 7. TEMs showing curved graphite sheet arrays for the cubic graphite phase produced by plasma-enhanced CVD. (**A**) Rectangle indicates the region of an off-axis view of the intersection of three spherical shells by high-resolution microscopy. (**B**) Micrograph showing the rectangular region in (A). (**C**) Magnified view of the rectangular region in (B). Arrows indicate an approximately 10-layer wall thickness. (**D** to **F**) Bright-field (D) and dark-field TEM images (E and F) of the same region. Insets in (E) and (F) show the arcs of the (002) ring that were used to produce the dark-field images. As the position of this arc was rotated, the areas of high intensity in the image also rotated, indicating that graphitic sheets are oriented parallel to the surfaces of the spheres.

ly, these graphite-tiled inverse opals are called cubic graphite. Like the proposed carbon phases called schwarzites, which were originally based on the tiling of triply periodic minimal surfaces with sheets of sp^2 carbons (*16*), the cubic graphite phase arises from tiling of the interior surface of the opal. However, unlike the proposed schwarzites, the present cubic graphite phase consists of graphitic sheets that are tiled upon each other—reminiscent of the structure of carbon onions (which are carbon particles consisting of concentric graphitic shells) (*15*). Moreover, this tiling of surfaces with graphite sheets is imperfect in the cubic graphite structure. On a dimensional scale that is a large fraction of the sphere diameter (where we cannot use high-resolution electron microscopy to image the individual graphite planes), we suspect that this tiling is like the overlapping layers of paper on a papier-mâché sphere.

Conclusion

The availability of carbon photonic crystals and the current synthesis methods have both fundamental and practical implications. For example, we are currently investigating the use of these carbon phases as templates for making composites and direct opals of thermoelectrics and electrostrictive materials (in which the figures of merit are optimized by the three-dimensional structure at optical and shorter wavelengths). Surface-templated inverse opals are particularly interesting for such multiple templating processes, because simple methods may be used to separately fill the interior and exterior void channels (Figs. 1B and 6) with different materials. Such void filling is analogous to the endohedral and exohedral doping of void space in fcc fullerenes like C_{60}. The inverse opals are also of particular interest as photonic band-gap materials, especially because a large volume fraction of the low refractive index phase facilitates gap formation (*1, 2*). The refractive index contrast for the diamond phase is not sufficient for formation of a complete gap for the diamond inverse opal. However, the combination of a low filling factor and high in-plane conductivity for the cubic graphite phase might lead to a plasmon-defined photonic band gap in the infrared region, which is at a much higher frequency than the recently found metallic photonic band-gap in the microwave region (*3*).

References and Notes

1. S. John, *Phys. Rev. Lett.* **58**, 2486 (1987); *Phys. Today* **44**(**5**), 32 (1991); K. Busch and S. John, *Phys. Rev. E.* **58**, 3896 (1998).
2. E. Yablonovitch, *Phys. Rev. Lett.* **58**, 2059 (1987); E. Yablonovitch and K. M. Leung, *Nature* **391**, 667 (1998).
3. D. F. Sievenpiper, M. E. Sickmiller, E. Yablonovitch, *Phys. Rev. Lett.* **76**, 2480 (1996); J. Joannopoulos, R. Meade, J. Winn, *Photonic Crystals* (Princeton Univ. Press, Princeton, NJ, 1995).
4. J. H. Holtz and S. A. Asher, *Nature* **389**, 829 (1997); A. van Blaaderen, R. Ruel, P. Wiltzius, *ibid.* **385**, 321 (1997).
5. A. P. Philipse, *J. Mater. Sci. Lett.* **8**, 1371 (1987); H. Míguez *et al., Appl. Phys. Lett.* **71**, 1148 (1997); C. López *et al., Superlattices Microstructures* **22**, 399 (1997).
6. V. N. Bogomolov, Y. A. Kumzerov, S. G. Romanov, V. V. Zhuravlev, *Physica C* **208**, 371 (1993); K. Yoshino, K. Tada, M. Ozaki, A. A. Zakhidov, R. H. Baughman, *Jpn. J. Appl. Phys.* **36**, L714 (1997); Y. A. Vlasov *et al., Phys. Rev. B* **55**, R13357 (1997); S. G. Romanov *et al., J. Cryst. Growth* **159**, 857 (1996); S. Tsunekawa *et al., Microporous Mater.* **8**, 275 (1997).
7. A. Imhof and D. J. Pine, *Nature* **389**, 948 (1997); O. D. Velev, T. A. Jede, R. F. Lobo, A. M. Lenhoff, *ibid.*, p. 447; B. T. Holland, C. F. Blanford, A. Stein, *Science* **281**, 538 (1998); J. E. G. Wijnhoven and W. L. Vos, *ibid.*, p. 802.
8. P. J. Darragh, A. J. Gaskin, J. V. Sanders, *Sci. Am.* **234** (no. 4), 84 (1976); N. D. Deniskina, D. V. Kalinin, L. K. Kazantseva, *Gem Quality Opals, Their Synthesis and Natural Genesis* (Nauka, Novosibirsk, 1988) [in Russian].
9. A. J. Gaskin and P. J. Darragh, U.S. Patent 3 497 367 (1970).
10. E. G. Acker and M. E. Winyall, U.S. Patent 4 049 781 (1977).
11. The following methods were used to obtain phenolic inverse opals and derivative glassy carbon inverse opals. A millimeter-thick slab of porous opal was immersed for 2 days in a bath of furfuryl-based phenolic resin (LP-520 FurCarb resin from QO Chemical, Inc., catalyzed by using trace HCl), which filled the opal with the resin. The resin was cured within the porous opal at temperatures between 80° and 130°C for 7 days. The opal was cut from the surrounding cured resin matrix, the opal was treated for 10 min in an oxygen plasma cleaner to remove residual surface phenolic, and the SiO_2 spheres in the opal were removed by exposure to 48% aqueous HF for 3 hours. This phenolic inverse opal was then carbonized to produce the glassy carbon inverse opal by heating under flowing argon for 1 hour at 900° to 1000°C.
12. V. G. Ralchenko *et al., Diamond Related Mater.* **6**, 159 (1997).
13. The diamond nuclei were seeded within the opal plates by ultrasonic agitation of these plates in an acetone suspension of 2- to 5-nm-diameter diamond grit. A microwave-plasma-enhanced chemical-vapor-deposition reactor (*12*) (operating at 2.45 GHz and 3.5 kW) was used to infiltrate carbon into the opals from a CH_4- and H_2-fed plasma (50 to 60 Torr pressure and gas flows of 972 sccm for H_2 and 25 sccm for CH_4). The deposition substrate temperature reached by plasma heating was 750° to 850°C and the deposition time was 64 hours. After the diamond surface of a carbon-infiltrated opal sheet was attached to a graphite plate substrate (using colloidal graphite paint), the SiO_2 spheres were removed by using a 1-day exposure to 10% HF, and the samples were repeatedly washed with water.
14. R. J. Nemanich, J. T. Glass, G. Lucovsky, R. E. Shroder, *J. Vac. Sci. Technol. A* **6**, 1783 (1988).
15. E. D. Obraztsova *et al., Carbon* **36**, 821 (1998).
16. A. L. Mackay and H. Terrones, *Nature* **352**, 762 (1991); T. Lenosky, X. Gonze, M. Teter, V. Esler, *ibid.* **355**, 333 (1992); D. Vanderbilt and J. Tersoff, *Phys. Rev Lett.* **68**, 511 (1992).

17. We thank K. Yoshino, V. Z. Vardeny, S. John, L.-M. Liu, I. Udod, A. Ribaudo, C. Bednarczyk, and I. U. Bakhadyrov for discussions and other valuable contributions. Partially supported by DARPA grant DAA-96-J-036 and a NEDO grant on Tunable Photonic Crystals. S.O.D. thanks the Brazilian agency CAPES for financial support as a visiting scholar.

11 June 1998; accepted 10 September 1998